Top-Down Cracking of Rigid Pavements Constructed With Fast Setting Hydraulic Cement Concrete

Andrew C. Heath* and Jeffery R. Roesler**

*Transportek, CSIR, PO Box 395, Pretoria, 0001, South Africa

** Pavement Research Center, Institute of Transportation Studies, University of California at Berkeley, 1353 S. 46th St, Bldg 480, Richmond, CA, 94804, USA.

Jointed Plain Concrete Pavement (JPCP) test sections were constructed using Fast Setting Hydraulic Cement Concrete (FSHCC) as part of the California accelerated pavement testing program (CAL/APT). Many of the longer slabs cracked under environmental influences before any traffic load was applied to them. Data from field instrumentation was recorded and analyzed along with laboratory test data to determine the cause of the cracking. Cores drilled through the cracks indicated that cracking initiated at the top of the slabs and propagated downwards. This was confirmed using the ILLI-SLAB (ILSL2) finite element package where high tensile stresses were predicted at the top of the slab as a result of the differential drying shrinkage between the top and base of the slab and the non-linear nature of the negative temperature gradients through the slab. Laboratory free shrinkage tests on the test section concrete indicated significantly higher shrinkage than an ordinary Type II Portland cement. Load plus environmental stress analysis with ILSL2 suggested the critical failure location for the FSHCC pavements would be near the corner of the slab not at the mid-slab edge.

INTRODUCTION

Most of the rigid pavements in urban areas in California have passed their design lives and are in various stages of distress. The agency and road user costs of applying lane closures in urban areas is very large compared to the actual costs of materials and placement.

To minimize lane closures, Caltrans proposed the use of Fast Setting Hydraulic Cement Concrete (FSHCC) to facilitate the reconstruction of urban freeways. Since little information was known about FSHCC pavement performance under loading and the environment, Caltrans initiated a research project to

design, construct, and test a full-scale field test section. Jointed Plain Concrete Pavement (JPCP) test sections were constructed using FSHCC along State Route 14 near Palmdale, California as part of the Caltrans Accelerated Pavement Testing program (CAL/APT). The testing and analysis of the project data was undertaken by the University of California at Berkeley, Dynatest Inc., and the CSIR from South Africa, in cooperation with Caltrans.

Several months after construction of the FSHCC pavement test sections, most of the longer test slabs had cracked under environmental influences, i.e., no traffic loading was applied. This paper presents an initial analysis into the failure of the slabs under environmental loading.

FIELD TEST SECTIONS

In June 1998, the concrete test sections were constructed by a contractor, with construction supervision by Caltrans. The test section slabs had varying dimensions, thickness, base types, and joint load transfer scenarios. Roesler et al. (*1*) lists the slab dimensions, thickness, and other pertinent information about the test sections. The test slabs were constructed for environmental monitoring and accelerated pavement testing using the Heavy Vehicle Simulator (HVS). The purposes of the HVS testing were to develop fatigue relationships for FSHCC pavements, evaluate proposed design features like dowels, widened lanes, and tied concrete shoulders, and monitor the joint performance of doweled and undoweled pavement sections (*2*).

Concrete Materials

The Fast Setting Hydraulic Cement Concrete (FSHCC) used in Palmdale was made up of two aggregate sizes, a blend of 80 percent Calcium Sulfoaluminate ($C\bar{S}A$) cement and 20 percent Type II Portland cement, and several chemical admixtures (*1*). Table 1 lists the mix design (stock) used by the contractor and the average flexural (ASTM C78) and compressive (ASTM C39) strengths of the FSHCC at 8 hours, 7 days, and 90 days.

The concrete surface was sprayed with a single layer of polymer-based curing compound after construction.

Instrumentation

An automatic data acquisition system and over 300 instruments were installed in the test sections prior to construction to enable data collection during and after construction. The instruments mainly used in the analysis of the environmental effects were multi-depth thermocouples, Carlson A-8 strain gages, and joint displacement measuring devices (JDMDs), as shown in Figure 1. Carlson A-8 strain gages measure the change in length of the concrete from temperature, shrinkage, and creep. Thermocouples measured the temperature of the concrete slab at different depths. JDMDs were used to measure the corner deflections of the slabs due to daily temperature variations. Data from these instruments, installed at various locations in the test sections, were recorded at least every 15 minutes during and immediately after construction and every two hours thereafter.

Weather Conditions

Palmdale, California has a desert type environment with extreme temperatures and fairly low rainfall and humidity. A weather station was installed at the site and weather data was automatically recorded every two hours. Mean monthly temperatures varied from 27.2 °C in August to 7.2 °C in December. Rainfall occurs mainly in winter and varied from 0.6 mm in July to 18.2 mm in January. The average monthly relative humidity varied between 30 and 55 percent.

Initial Concrete Test Section Performance

After two months of exposure to the desert environment, 37 out of 74 slabs in the test sections cracked under environmental conditions before any traffic loading was applied. These transverse environmental cracks typically ran through the center of the slab, as illustrated in Figure 2.

The variable joint spacing used on the test section slabs was on average 3.66, 3.96, 5.49, and 5.79 m. All transverse cracks occurred on slabs with long joint spacing (5.49 and 5.79 m slabs). Initial theoretical analysis using only temperature effects indicated excessive daytime curling stresses, which would result in maximum tensile stresses at the bottom of the slab. This tensile curling stress would cause crack initiation at the bottom of the slab and crack propagation from the bottom to the top of the slab. However, cores drilled through the surface cracks revealed cracks began at the top and propagated down to the bottom of

the slab, but not necessarily full-depth, as shown in Figure 2. High daytime temperature curling could therefore not be the primary cause of the cracking.

In order to determine the cause of the cracking, field instrumentation data was analyzed and laboratory testing was performed to determine the concrete's free shrinkage and coefficient of thermal expansion.

FIELD TEST DATA

Figure 3 shows the net effect of concrete thermal contraction after construction, plastic and drying shrinkage, and creep in the 200 mm test slabs. This is the average response for all slabs, as determined by the Carlson A-8 strain gages located 40 mm from the top and bottom of the slabs. As shown in Figure 3, the top and bottom of the slab contracted at similar rates during the first few days after construction. There was little strain differential between the top and base of the slab during this period, and therefore no stresses or cracking from bending or curling would be expected. The maximum measured concrete strain differential through the slab (approximately 150 με) occurred 2-3 months after construction which is in the time period where transverse cracking was first observed.

Temperature effects

The temperature effects were assessed using the thermocouples installed at various depths in the pavement, the joint displacement measuring devices (JDMD) installed at the corners of several slabs, and the A-8 strain gages installed in the slabs.

The temperatures during and after construction were measured for the different slabs using thermocouple stacks positioned at various locations in the slabs (edge, corner and center). Temperature data taken during construction for a 200 mm slab poured at approximately 14:00 (heat of the day) resulted in a maximum temperature of approximately 40°C and a maximum temperature differential of 5°C, both occurring at approximately 16:00.

The average post-construction temperature differential for the 200 mm slabs at 16:00 was 6.5°C, slightly above the maximum differential of 5°C immediately after construction. The differential strain caused by the differential concrete cooling was determined to be small (12με) compared to the magnitude of differential strain measured a few months after construction (see Figure 3).

The uniform cooling of the slab to ambient temperatures after construction (from 40°C to 25°C) would have caused axial contraction which would have occurred during the first few days after construction. This

can be seen in Figure 3 where both the top and bottom strains increase at similar rates during the first few days after paving. With the available data, it is difficult to separate the thermal effects, concrete shrinkage and creep during this period although it is likely that thermal contraction is the major component of the measured strain. If the slabs were restrained by base friction or bonding to the adjacent slabs, thermal contraction cracking would have occurred in the first few days after construction when the majority of the thermal contraction occurred. As seen in Figure 3, the strains at the top and bottom of the slab were affected by the cooling and heating during winter and spring, respectively. The average slab temperature changed from 30.0°C to 9.3°C during this period. As the slab uniformly cooled down and heated up, this caused contraction and expansion of the slab which would not have affected the curling stresses. The contraction during winter would add to the axial stresses, if the slabs were restrained against movement.

Since the differential concrete strains took three months to develop the maximum value, it was concluded that thermal effects caused by warm weather paving were not the primary cause of these cracks.

Concrete drying shrinkage

Since thermal contraction of the concrete was not the primary cause of the differential strains through the slabs, differential concrete drying shrinkage was the most plausible reason. As shown in Figure 3, the top of the slab experienced more drying shrinkage than the base of the slab, which is consistent with previous observations (*3,4*). This is because the top of the slab is exposed to lower humidity, wind, and higher temperatures, and therefore has a higher evaporation rate than the bottom of the slab. Previous researchers (*3,4*) have indicated little to near zero drying shrinkage below the mid-depth of the slab. Figure 3, shows significant concrete contraction near the base of the slab immediately after construction and again going into the winter months. As discussed previously, this can be attributed to thermal effects and the drying shrinkage data therefore appears to agree with the previous experience.

The slight reduction in the differential shrinkage through the slab with time can be explained by drying out of the bottom of the slab, an increase in moisture content at the top of the slab during the wet season, and/or concrete creep with time (relaxation of top strain).

LABORATORY TEST DATA

In order to verify the field shrinkage findings and the concrete coefficient of thermal expansion, laboratory tests were performed on the concrete materials used in the construction of the test sections and on several other concrete materials used in California. These laboratory tests were needed first to compare FSHCC to ordinary PCC and to obtain material data required for a stress analysis of the pavement test sections.

Coefficient of thermal expansion

In order to assess the influence of temperature on environmental stresses, the concrete coefficient of thermal expansion, α, was required. This was determined using both a modified form of ASTM method C 531-85 and United States Army Corps of Engineers (USACE) test method CRD-C 39-81.

The mean coefficient of thermal expansion from all the tests was 8.1E-06 / °C with a standard deviation of 6.5E-07 / °C. There were no appreciable differences between the values obtained for different curing times (28 and 90 days), curing conditions (wet and dry), and test methods. Previous research has shown that the aggregate type has more of an effect on α for concrete than any of these above factors (*5*). The Gabbro coarse aggregate used in the construction of the test sections (Table 1) has a slightly lower α than most other common aggregate types.

Drying Shrinkage

The drying shrinkage of the cement paste and concrete was assessed using a number of test methods and curing conditions. The shrinkage of mortar bars was assessed using California test CT 527 (similar to ASTM C 596-96) and the shrinkage of concrete beams was assessed using a slightly modified version of ASTM C 157-93.

Mortar Bar Shrinkage Test

The shrinkage of the $C\bar{s}A$ and Type II blend ($C\bar{s}A1$), used in the construction of the Palmdale test sections, a new blend of $C\bar{s}A1$, a $C\bar{s}A$ cement from another manufacturer ($C\bar{s}A2$), a Type III with calcium chloride ($CaCl_2$), and a Type II cement are shown in Figure 4.

These results are only given as relative comparison as many factors influence the shrinkage of concrete in the field. The shrinkage of the Type II mortar can be used as a relative standard for typical concrete pavements.

As shown in the figure, the $C\bar{s}A1$ cement used in the construction of the test sections and the Type III with $CaCl_2$ had the highest shrinkage. High shrinkage is not necessarily a feature of $C\bar{s}A$ cements, as the unblended $C\bar{s}A2$ cement and new blend of $C\bar{s}A1$ had the lowest free shrinkage. Drying shrinkage has not been a typically problem with pavements constructed with Type II cement in California. However, Type III with $CaCl_2$ has been known to exhibit early age shrinkage cracking similar to that observed in the Palmdale test sections with $C\bar{s}A1$. As shown with the shrinkage tests in the laboratory, cements with significantly greater shrinkage than Type II cements have shown cracking potential when used in concrete pavements in California.

Concrete Shrinkage Tests

The shrinkage of the concrete and mortar bars with a 0.40 water to cement ratio are shown in Figure 5. As shown, the concrete made with the $C\bar{s}A$ blend had a higher ultimate shrinkage than the concrete made with the Type II cement. The $C\bar{s}A$ and Type II cements had similar concrete shrinkage at 7 days. After 7 days, the $C\bar{s}A$ concrete increased in shrinkage at a much high rate than the Type II concrete. By 90 days, the $C\bar{s}A$ concrete had 33 percent more shrinkage than the Type II concrete. The concrete shrinkage had not peaked off after 90 days curing, probably due to the larger sample dimensions. The data for the concrete shrinkage had more scatter than for the mortar bars, probably as a result of the varying humidity and larger cross-sectional area. The free shrinkage strains measured for the concrete or mortar are not directly applicable to field concrete slabs, but do give an indication of relative performance in the field.

CONCRETE PAVEMENT ANALYSIS UNDER ENVIRONMENTAL LOADING

To verify cracking in the slab was by differential shrinkage and temperature curling, finite element analysis was conducted with an existing rigid pavement analysis program. The pavement response to a number of different parameters was investigated using the ILSL2 finite element package, which was developed by Khazanovich (*6*). ILSL2 is an updated version of the ILLI-SLAB program (*7*). Several key

features of ILSL2 are the ability to analyze generalized non-linear slab temperature distributions and layer separation.

The slab's elastic modulus (35 GPa) and the modulus of subgrade reaction (150 MN/m^3) were back-calculated from Heavy Weight Deflectometer (HWD) data (*1*) and were used as inputs in this analysis.

The warping from differential shrinkage was modeled using a bi-linear shrinkage model, similar to that used in the HIPERPAV software for analyzing the early age behavior of jointed concrete pavements (*3*). The HIPERPAV software assumes the maximum shrinkage occurs at the surface of the slab with a decrease to zero shrinkage below the slab's mid-depth. Based on the measured strains in the field, this assumption appears to be reasonable. In this analysis, the maximum measured differential shrinkage of approximately 150 με (Figure 3) was increased to 250 με, as the measured differential was determined from strain gages positioned 40 mm from the top and bottom of the slab, respectively. This value of 250 με was assumed to occur at the slab surface with a uniform shrinkage assumed below the slab mid-depth. The shrinkage profile was converted into an equivalent temperature distribution and added to the actual non-linear temperature distribution. In this analysis, the friction between the concrete and cement treated base layer and possible bonding to adjacent slabs was not considered, even though this can have significant effects on the slab stresses (*8*).

Corner deflections

The displacements of several slabs under daily temperature cycles were assessed using the Carlson A-8 and JDMD data for strains and displacements and thermocouple data for the in-slab temperatures. The relationship between slab temperature differential and JDMD and A-8 data during a typical daily temperature cycle is shown in Figure 6.

The data was corrected to a zero reading at the lowest point that the slab corner reached during the day in question. As shown in the figure, the slab corners moved approximately 2.5 mm in a vertical direction during the daily temperature cycle. There is a hysteresis to the loop, which is a result of the non-linear nature of the temperature distributions in the slab. The JDMD data indicated that the slab corners may not have come into complete contact with the base during the day. If the corners did touch the ground while there was a positive temperature gradient, the JDMD data would probably be more like the predicted values shown on the chart, as the corners would push slightly into the ground surface while the center of the slab

lifted into the air. As the data does not show this trend, the shrinkage differential through the slab must have been sufficient to keep the corners unsupported even at the maximum daytime temperature differential. This curled up condition has significant implications for critical traffic load locations.

The slab corner deflections were calculated using the temperature gradients measured from the thermocouple stacks and the average laboratory coefficient of thermal expansion of 8.1E-06 / °C. A 3.66 m x 3.96 m and 200 mm thick slab was used in the analysis as this slab had not cracked under environmental influences.

Figure 7 shows the predicted corner deflections at different time during a typical day compared to the JDMD reading for the corner of the same slab. The finite element analysis (FEA) closely predicts the slab corner deflections given the slab's temperature and shrinkage profile. If the differential shrinkage through the slab is ignored in the analysis, the slab corner deflections will be grossly underestimated, as seen in Figure 8. Yu et al (*9*) noted that built in upward curl was necessary to correctly match field corner deflections with FEA results.

The predicted FEA corner deflections had to be shifted forward by approximately 30 minutes in order to match the measured JDMD deflections. One possible reason for the time lag is the slab takes some finite time to reach equilibrium given a certain temperature profile, especially when the temperature profile is changing more rapidly during the middle of the day. The results of this temperature plus shrinkage analysis indicated that the corners of the slab did not achieve full contact with the subgrade in the day in question, i.e., the slab was curled upward even at the maximum daytime temperature gradient.

Concrete stresses

Besides the deflections, the concrete stresses were determined using ILSL2. It was found that although the largest temperature gradients occurred during the day, the highest concrete tensile stresses developed at the top of the slab under the extreme negative temperature gradients through the slab (during the night). This is because the shrinkage differential through the slab and the non-linear night time temperature gradients both increase the tensile stresses at the top of the slab. Previous research has indicated that the lowest concrete strengths occur at the surface of the slab as a result of poor curing conditions(*10*). As the highest concrete stresses and lowest strengths occur at the surface of a slab, crack initiation at the top of the slab and propagation downward is the most likely scenario.

The concrete stresses at the top of two different size slabs are shown in Figure 8. These stresses were determined under the maximum shrinkage differential (250με) and the worst case negative temperature gradient measured at Palmdale.

The worst case negative temperature gradient occurred at roughly the same time as the maximum shrinkage differential. The slab dimensions were 5.8 m or 4.0 m long, 3.8 m wide, and 200 mm thick for the analysis. The modulus of subgrade reaction, k, was 150 MN/m^3 and the concrete's elastic modulus was 35 GPa. As shown in Figure 8, the maximum tensile stresses are in the center of the slab, where the environmental cracking occurred. The maximum stress for the longer (5.8 m) slabs was approximately 13 percent above the flexural strength of the concrete (5.14 MPa). The maximum stress in the shorter (4 m) slabs was 23 percent lower than for the longer slabs and below the concrete flexural strength. This explains why the longer slabs cracked under environmental influences while the shorter slabs remained largely uncracked.

If the worst case environmental loading and a 40 KN dual wheel load (half a standard axle) are applied simultaneously, the critical load condition is for corner loading. The stresses for this situation are shown in Figure 9, where the maximum tensile stress for the longer slabs is significantly higher than the average flexural strength of the concrete. The stresses for the shorter slabs were again lower than for the longer slabs, but high enough to cause cracking when wheel loading is applied. Yu et al. (*9*) found similar stress results for certain concrete slab lengths and initially curled upward slabs. The stresses for the mid-slab edge loading case with a positive temperature gradient and no shrinkage gradient (often used in rigid pavement stress analysis) were approximately 40 percent lower than for corner loading case.

Based on the stress distribution patterns in Figure 9, loading of these slabs with half an axle may cause the failure mode to be corner cracking instead of the traditional transverse fatigue crack. Corner cracking was the typical failure mode for the Palmdale test slabs when subjected to accelerated pavement testing with the HVS (half an axle). Finite element analysis with a full axle indicated either corner or longitudinal cracking as the most likely mode of failure.

Further analysis revealed that the critical load location moves from the corner of the slab to the mid-edge at lower shrinkage differentials (less than 60 με in this case). The shrinkage differential at which this

occurs is not unique and is highly dependent on the slab dimensions, concrete modulus, and subgrade k-value.

CONCLUSIONS

The transverse cracking of Jointed Plain Concrete Pavement (JPCP) test slabs under environmental loading was investigated. The test slabs were constructed with Fast Setting Hydraulic Cement Concrete (FSHCC) in Palmdale, California as part of the Caltrans accelerated pavement testing program (CAL/APT). Cores drilled above the transverse cracking indicated top-down cracking had occurred.

The shrinkage and thermal properties of in-situ concrete pavements were monitored with strain gages, multi-depth thermocouples, and Joint Displacement Measuring Devices (JDMDs). Initial strains in the slab were most likely due to thermal contraction of the concrete after construction. After two months, strains at the top of the slabs had increased significantly while the strains measured in the bottom of the slab remained constant. It was determined that this increase in the top of slab was a result of drying shrinkage, not thermal contraction. The differential strains through the slab thickness resulted in slab bending stresses, which exceeded the concrete strength and caused transverse cracking. Laboratory testing performed on the cement ($C\bar{S}A$) and concrete used in the Palmdale test sections showed much higher free shrinkage relative to ordinary Type II Portland cement and reinforced the findings of the strain measurements.

JDMDs showed significant corner curling of the field concrete slabs, with as much as 2.5 mm daily movement under environmental conditions. The corner deflection data suggested the slab corners were permanently curled upward caused by the differential drying shrinkage in the slab.

An analysis of the slab corner deflections was performed by comparing the measured to predicted values from finite element analyses (ILSL2) using non-linear slab temperature profiles and drying shrinkage differentials. The corner deflections were accurately modeled provided the drying shrinkage differential was included in the analysis. The measured data and FEA showed the corners of the slab had significantly curled up due to differential drying shrinkage, resulting in an unsupported corner condition at all times.

By analyzing the differential shrinkage and a negative temperature distribution, the highest tensile stresses from environmental loading were found to be at the middle of the slab at the surface. This validated the field findings that crack initiation began at the top of the slab and propagated downward.

Load plus environmental stress analysis, showed excessive differential drying shrinkage resulted in the critical failure location being at the corner of the slab instead of at the mid-slab edge. This indicates either corner or longitudinal cracking as failure modes.

Using the analysis procedure in this paper, the critical load location and failure mode will be slab edge loading and bottom-up transverse cracking for concrete pavements with low shrinkage differentials, as typically observed with pavements constructed with Type II cement in California. The use of FSHCC does not necessarily indicate high shrinkage differentials as laboratory testing indicated some $C\bar{s}A$ cements can have lower shrinkage than Type II cements.

REFERENCES

1. Roesler, J R, Scheffy, C W, Ali, A and Bush, D. 1999. *Construction, Instrumentation, and testing of Fast-Setting Hydraulic Cement Concrete in Palmdale, California.* University of California at Berkeley, Berkeley, California.
2. University of California at Berkeley, Dynatest Consulting Inc., and CSIR, Division of Roads and Transport Technology, *Test Plan for CAL/APT Goal LLPRS—Rigid Phase III,* Prepared for California Department of Transportation, April 1998.
3. Rasmussen, R O and McCullough, B F. 1998. *A Foundation for High Performance Jointed Concrete Pavement Design and Construction Guidelines.* Transtec consultants, Austin, Texas.
4. Eisenmann, J and Leykauf G. 1990. Simplified Calculation Method of Slab Curling Caused by Surface Shrinkage. *Proceedings: 2nd International Workshop on the Theoretical Design of Concrete Pavements.* Spain.
5. Tia, M; Bloomquist, D; Alungbe, G D and Richardson D. 1991. *Coefficient of Thermal Expansion of Concrete used in Florida.* Department of Civil Engineering, University of Florida, Gainesville.
6. Khazanovich, L. 1994. *Structural Analysis of Multi-Layered Concrete Pavement Systems.* Ph.D. thesis, University of Illinois at Urbana-Champaign, Urbana, Illinois.
7. Tabatabaie-Raissi, A M. 1977, *Structural Analysis of Concrete Pavement Joints*, Ph.D Thesis, University of Illinois, Urbana-Champaign, IL.

8. Wimsatt, A W; McCullough, B F and Burns, N H. 1987. *Methods of Analyzing and Influencing Frictional Effects of Subbases.* Research Report 459-2F, Center for Transportation Research, University of Texas, Austin.

9. Yu, H T; Khazanovich, L; Darter, M I and Ardani, A. 1998. Analysis of Concrete Pavement Responses to Temperature and Wheel Loads Measured from Instrumented Slabs. *Proceedings: Transportation Research Board, 77th Annual Meeting* Washington, DC.

10. McCullough, D F and Dossey, T. 1999. Considerations for High Performance Concrete Paving : Recommendations from 20 Years of Field Experience in Texas. *Proc. Transportation Research Board Annual Meeting.* Washington, D.C. January 1999.

TABLE 1 Concrete stock weights and strengths

FSHCC Mix constituents		Batch weight (kg/m^3)
25 mm coarse Gabbro aggregate		1080
Fine Quartz aggregate		848
C$\bar{S}$A cement blend		332
Type II portland cement		83
Water		117
Delvo® stabilizer (ml/m^3)		95.5
Micro-Air® air entraining agent (ml/m^3)		1.36
Total water-to-cement ratio		0.39
Time after finishing	Ave flexural strength (MPa)	Ave compressive Strength (MPa)
8 hours	2.09	13.57
7 days	4.03	28.68
90 days	5.14	45.50

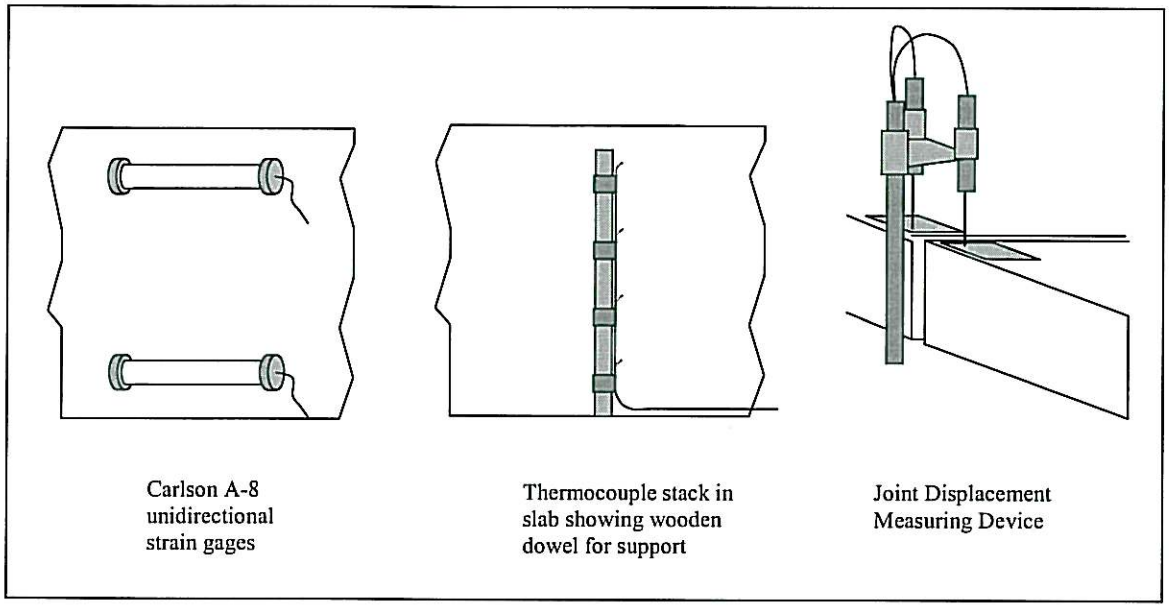

FIGURE 1 Instrumentation used to assess environmental loading effects

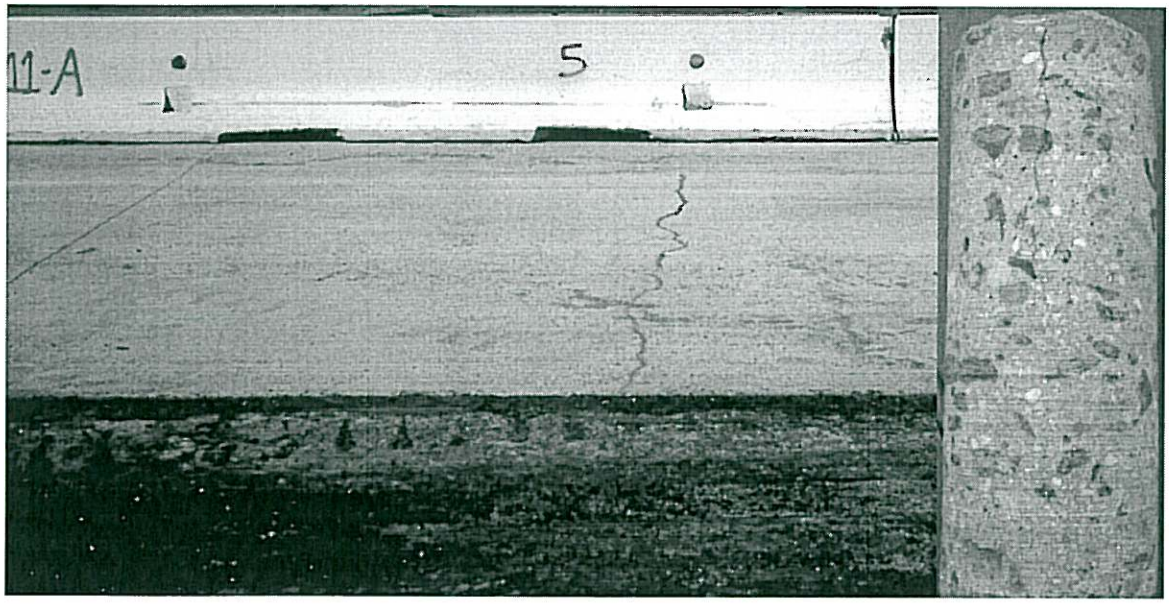

FIGURE 2 **Environmental crack through the center of a pavement slab and core through an environmental crack showing top-down cracking**

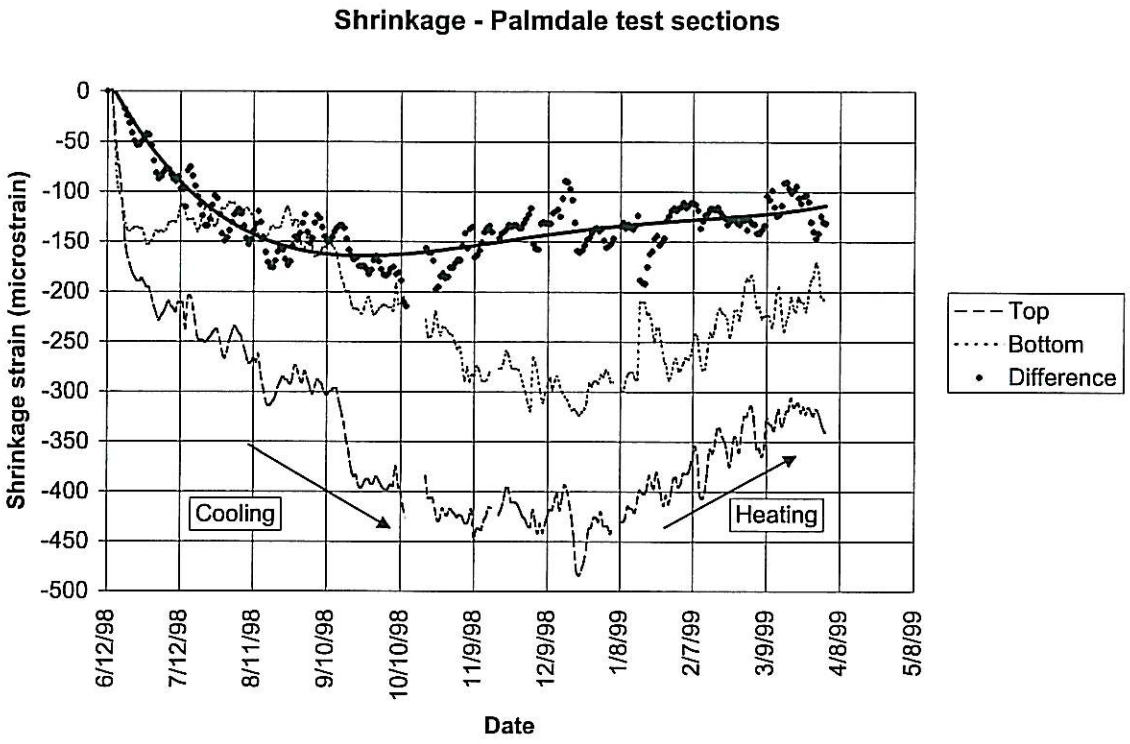

FIGURE 3 **Net concrete strain measured using Carlson A-8 strain gages**

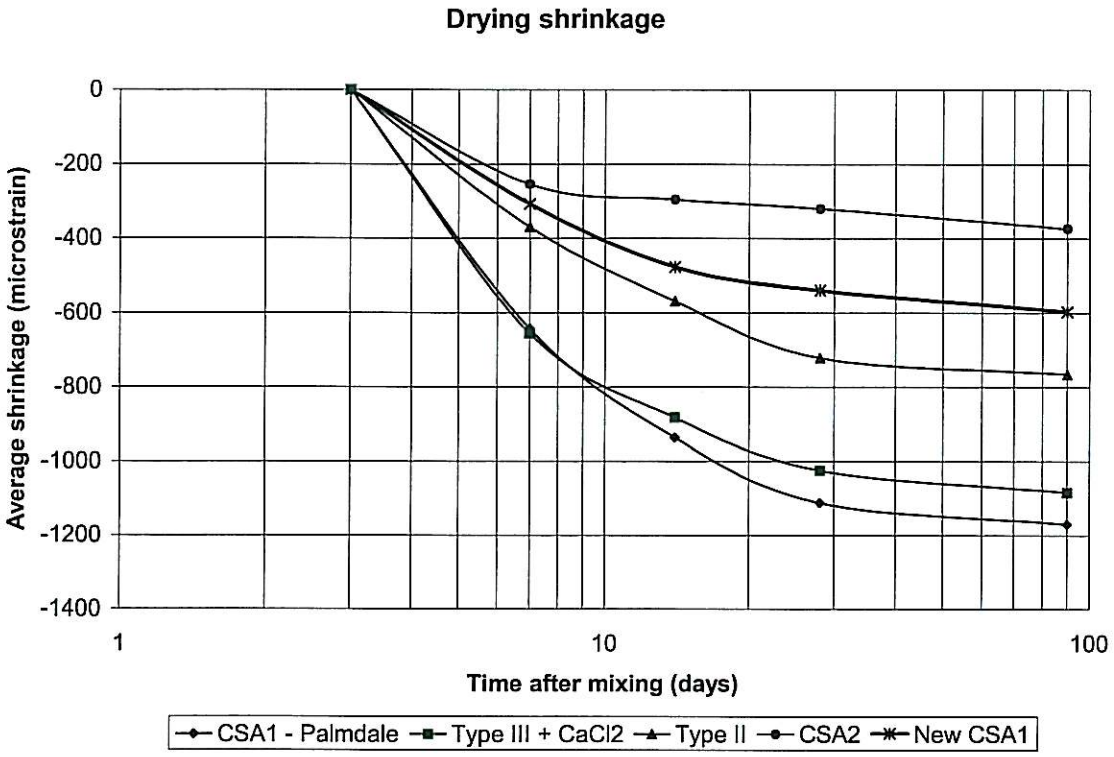

FIGURE 4 **Shrinkage of mortar bars at 20 °C and 50% relative humidity**

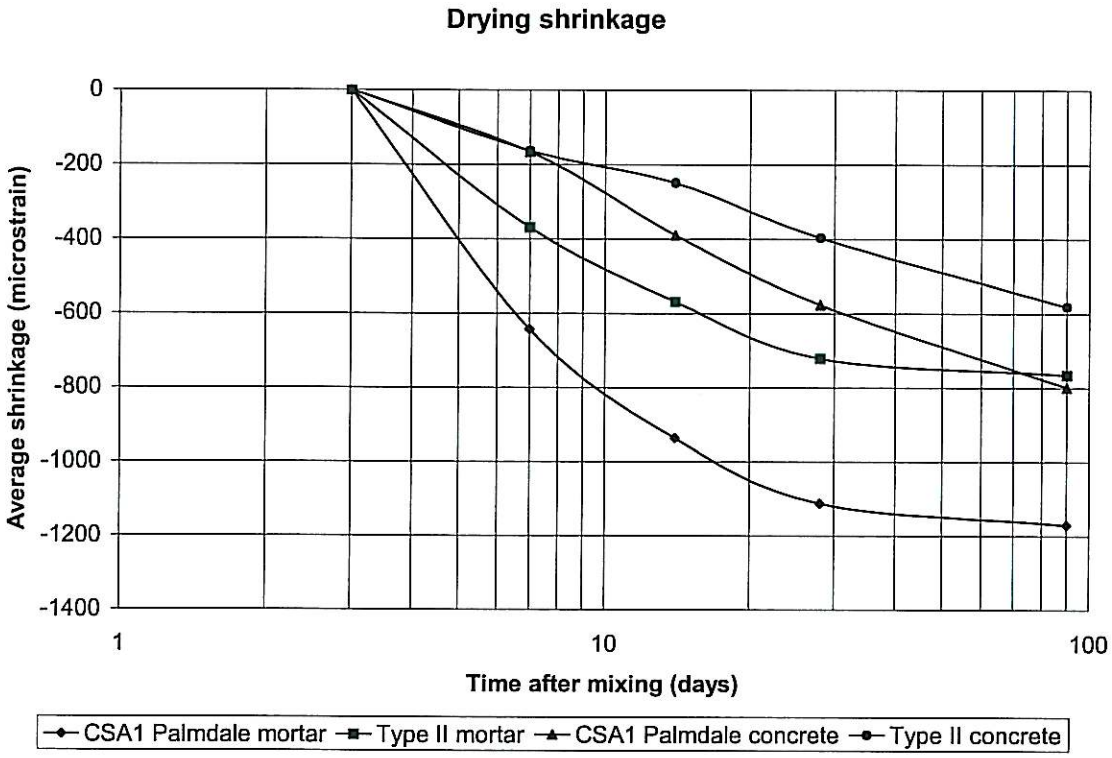

FIGURE 5 **Shrinkage of concrete and mortar bars**

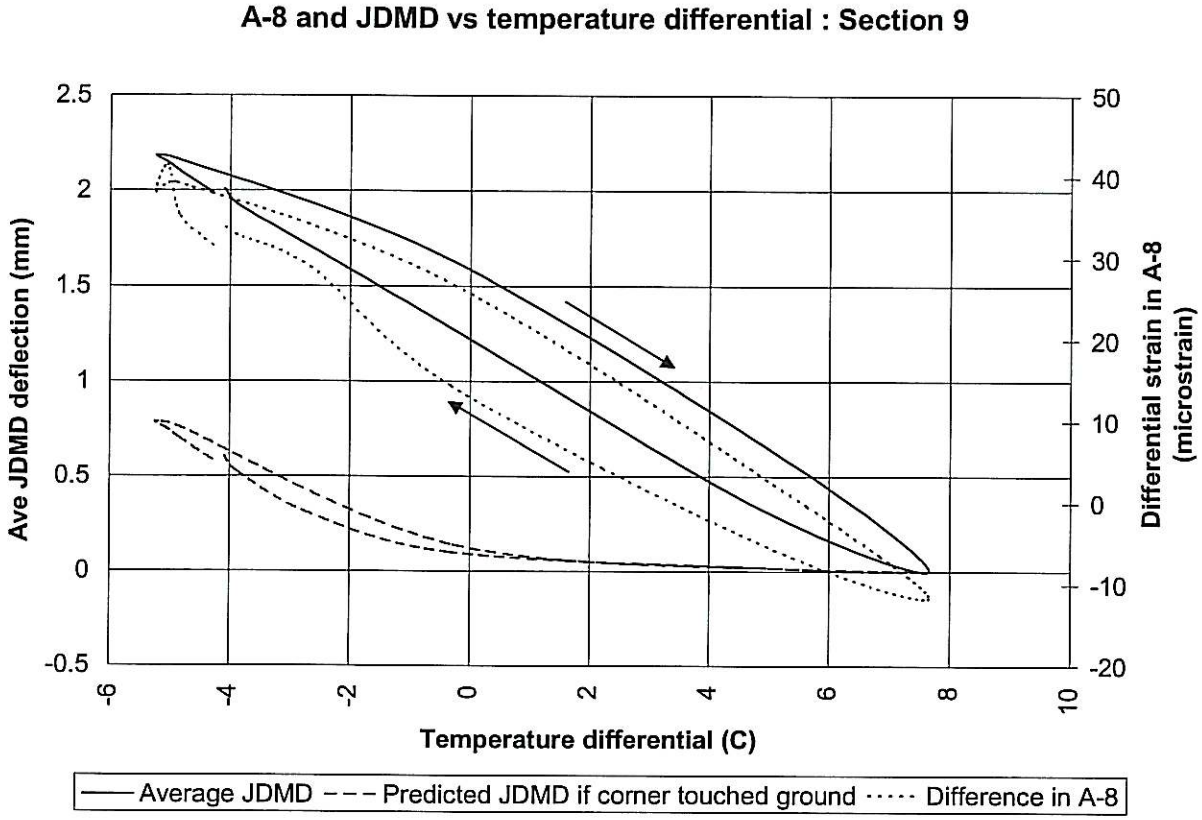

FIGURE 6 **Typical JDMD and A-8 data vs slab temperature differential**

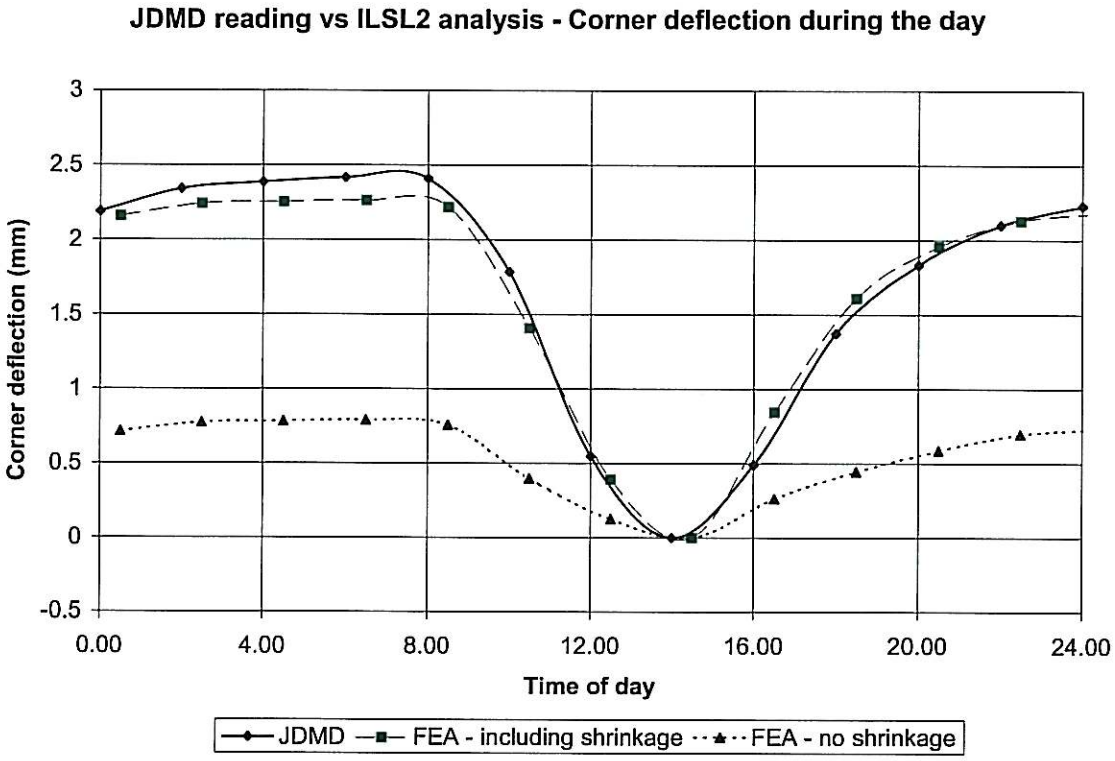

FIGURE 7 **JDMD reading vs finite element prediction**

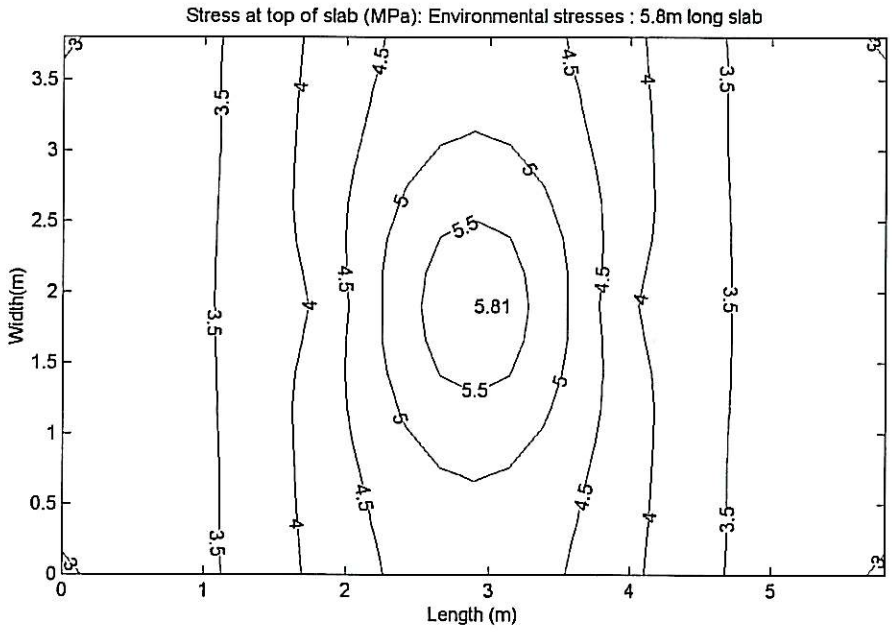

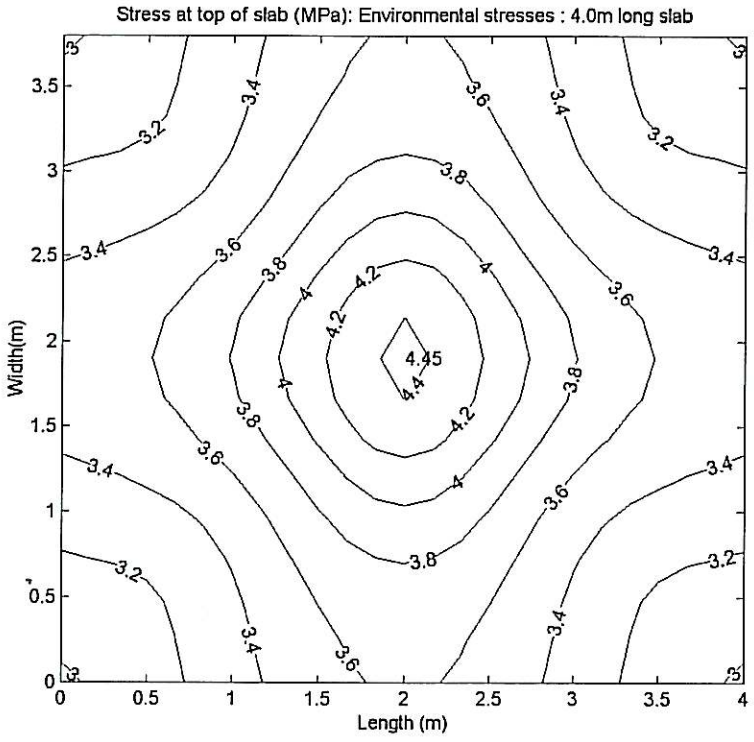

FIGURE 8 **Top of slab tensile stresses (MPa) under worst case environmental loading, top for 5.8 m and bottom for 4.0 m long slab**

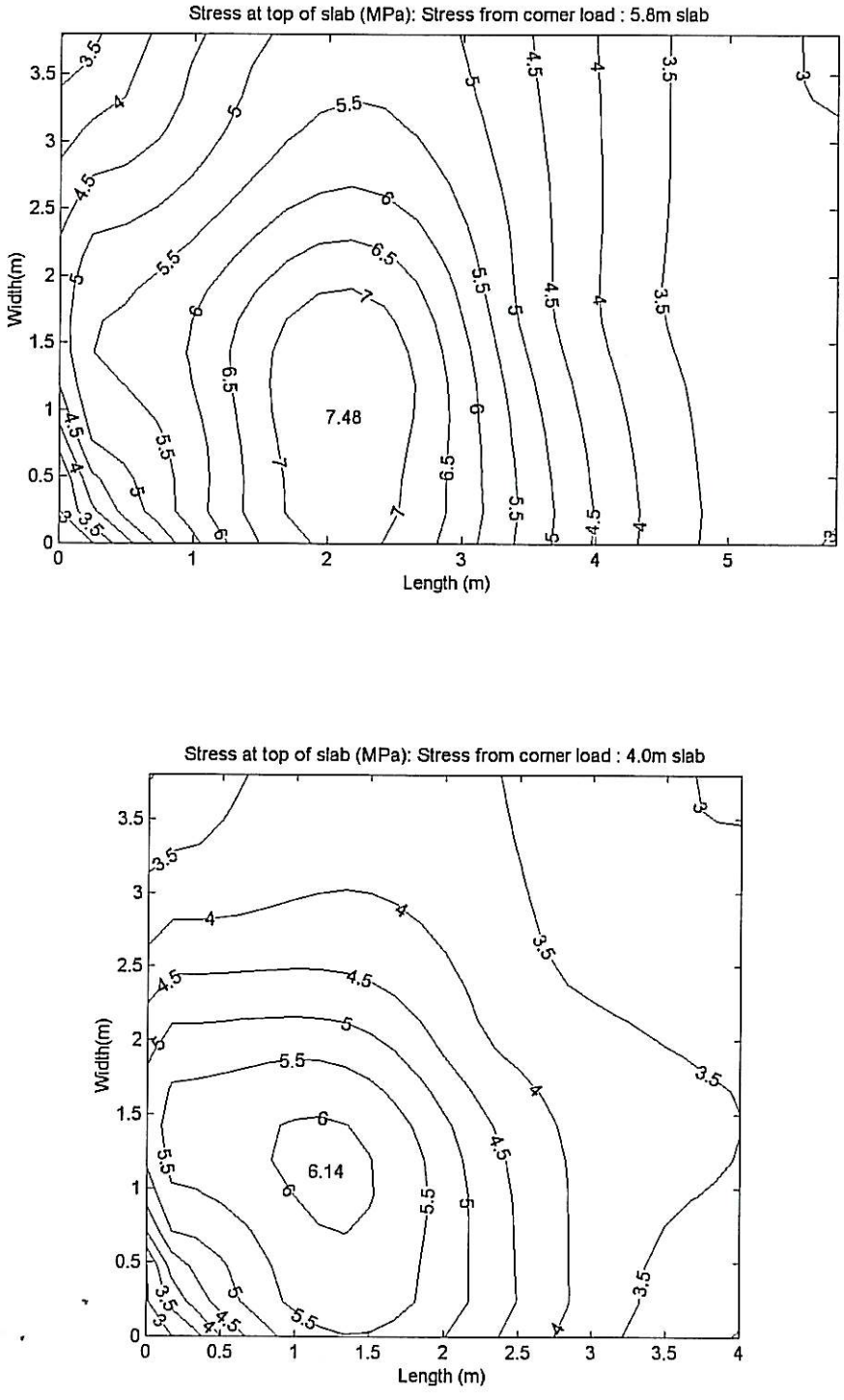

FIGURE 9 **Top of slab tensile stresses (MPa) under worst case environmental and 40 kN corner load, top for 5.8 m and bottom for 4.0 m long slab**